ELSEVIER

Chemical Engineering Journal 140 (2008) 578–585

Chemical Engineering Journal

www.elsevier.com/locate/cej

# Mathematical modeling of the generation of the secondary porous structure in a monolithic adsorbent

B. Ledvinkova [a], F. Keller [b], J. Kosek [a,*], U. Nieken [b]

[a] *Department of Chemical Engineering, Institute of Chemical Technology Prague, Technicka 5, 16628 Prague 6, Czech Republic*

[b] *Institut für Chemische Verfahrenstechnik, Universität Stuttgart, Böblinger Str. 72, 70199 Stuttgart, Germany*

Received 3 May 2007; received in revised form 1 February 2008; accepted 5 February 2008

**Abstract**

Monolithic adsorbent structures are of interest in pressure-swing adsorption due to its low pressure drop and mechanical stability in order to prevent attrition. We consider a monolithic adsorbent consisting of micro-porous zeolite particles embedded in a polyamide matrix. After the extrusion of a zeolite filled polyamide matrix a secondary structure of transport pores has to be formed in the polyamide phase to allow fast mass transport of the adsorbate to the zeolite particles. Here we develop a proof-of-the-concept mathematical model to describe the generation of the macro-porous structure in a zeolite–polyamide–wax system. The mathematical model is based on the discrete element method (DEM). We demonstrate that the problem of evolution of a complex morphology can be modeled by the DEM model. Systematic parametric studies provide us with the qualitative guidance on the effects of processing parameters and the initial distribution of polyamide and wax phases on the final morphology of the monolithic adsorbent.



*Keywords:* Monolithic adsorbent; Generation of porous structure; Discrete element method

## 1. Introduction

Monolithic adsorbents consist of an adsorbate, for instance zeolite particles, and a matrix material, usually either a ceramic material or – in our case – a polymeric material such as polyamide. Manufacturing of these materials is a two-stage process. In the first stage the monolithic structure of parallel channels of square cross-section is extruded from a suspension of polyamide and a fine zeolite powder. In order to adjust the viscosity of the melt and to improve the extrusion process a wax is added. The micro-mixing of polyamide and wax phases is not perfect, therefore the solid-phase of the extruded monolith contains three phases: zeolite, polyamide and wax, cf. Fig. 1. The second stage in the production of monolithic adsorbents is the generation of a secondary macro-porous structure to improve mass transport to the embedded zeolite crystals. The generation of transport pores in polyamide therefore magnifies the adsorption kinetic, which is essential for pressure-swing adsorption, while maintaining high stability and good embedding of zeolite particles in the polyamide matrix [1].

The comparison of the adsorptive properties of the monolith with and without secondary pore structure was experimentally realized by Fritz and Hammer [2]. The reported mass transfer coefficients of the monoliths were normalized with the result of commercial zeolite 4A granules (Grace Davison Chemicals SP7-8374.518, 15 mm pellets). Before the thermal treatment, i.e., in the monolith without the secondary pores, the adsorption kinetics is retarded in comparison to zeolite A4 powder, represented by a normalized mass transfer coefficient of 0.5 [3]. The non-zero value of the mass transfer coefficient in this case is attributed to the adsorption capacity of accessible pores of zeolite particles and diffusion through the polymer. After the thermal treatment and the development of the secondary pore structure, the adsorber monolith shows a remarkable improvement in the adsorption kinetics by a factor of 4 when compared to the reference zeolite pellets. The monolith containing secondary pores exhibits an order of mangnitude increase in the mass transfer coefficient. Zeolite particles are not distributed uniformly within the polyamide phase as they form small agglomerates in the polymer framework. By adding short-chained wax the wetting of the

* Corresponding author. Tel.: +420 220 44 3296; fax: +420 220 44 4320.
*E-mail address:* Juraj.Kosek@vscht.cz (J. Kosek).

1385-8947/$ – see front matter © 2008 Elsevier B.V. All rights reserved.
doi:10.1016/j.cej.2008.02.008

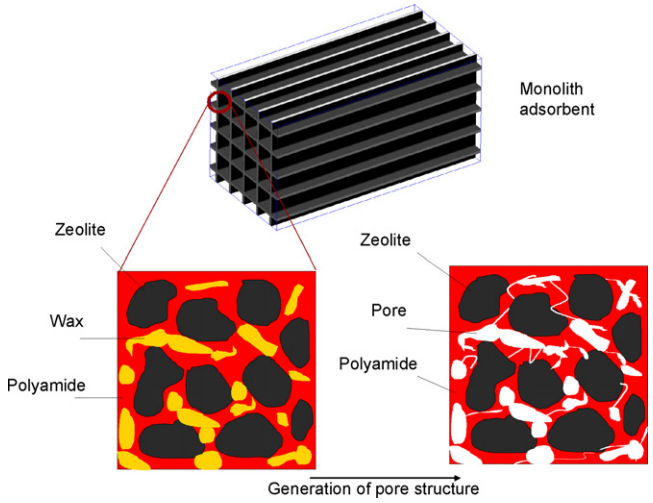


Fig. 1. Generation of the secondary porous structure in the solid-phase of monolithic adsorbent.

zeolite is increased compared to the high molecular polyamide, thereby enhancing the mixing of zeolite in the polymer matrix.

## 2. Adsorption monolith and the generation of its structure

The monolith is either block or cylinder containing 200 channels per square inch. The width of one channel is approximately 1.5 mm. The solid-phase of monolith is composed from 55 to 70 wt.% of porous zeolite particles (e.g., SP 565-10062) with the diameter 1–10 μm. The estimated diameter of primary pores in zeolite is in the range of nanometers. Due to the high content of zeolite in the monolith structure a tight packing of zeolite particles is assumed. Thus a limited transport of gas molecules can occur between touching zeolite particles.

In the first stage of manufacturing the melt consists of 55–70 wt.% of zeolite as mentioned previously, 20–35 wt.% of a polyamide phase (Polyamide 6,6—Ultramid A3SK) and a wax content of 5–20 wt.%. The wax is either a mixture of polyolefins and polyglycol (Licomont EK 583) or a pure polyglycol (Polyglykol 20000). The morphology of the mixture of polyamide and wax in the extruded monolith is unknown, but we assume that the wax phase is distributed within the polyamide phase in small islands. These wax islands can be linked together to form a pseudo-continuous phase due to the large weight ratio of wax to polyamide.

The generation of the secondary porous structure in the second stage of adsorption monolith manufacturing consists in removing of the wax phase. Two ways of wax removal were tested: the first one is the extraction of wax by suitable solvents and the second one is the thermal decomposition of wax [4]. The extraction process by various solvents (e.g., ethanol and acetone) is a very time consuming process with low efficiency. The second way of wax removal is realized by heating of the monolith in an oven. It utilizes different temperatures of decomposition of the low molecular weight wax (180 °C) and high molecular weight polyamide (240 °C). The monolith is therefore heated in the oven to the temperature of 180–200 °C. The time of monolith treatment in the oven depends on the amount and on the distribution of wax in the monolith and varies between 6 and 24 h. The treatment of the monolith in the oven provides considerably better results with respect to the generation of the pore structure than the removal of wax by extraction.

The problem of the monolith treatment in the oven is the possible overheating of the monolith. Local temperatures of 250 °C can be reached [4]. The reason for overheating is oxidation of wax in the stream of air compared to a slow removal of the reaction heat. The overheating can cause the inflammation of the polymer matrix and thus its damage. This hypothesis has been confirmed by the monolith treatment in the oven with the inert gas added to the stream of air, where the overheating manifested by a dark color of the treated adsorbent was not observed [4]. Nevertheless careful oxidation of the wax phase allows the generation of a secondary pore structure without loss of mechanical stability. Scanning electron microscopy (SEM) pictures of the

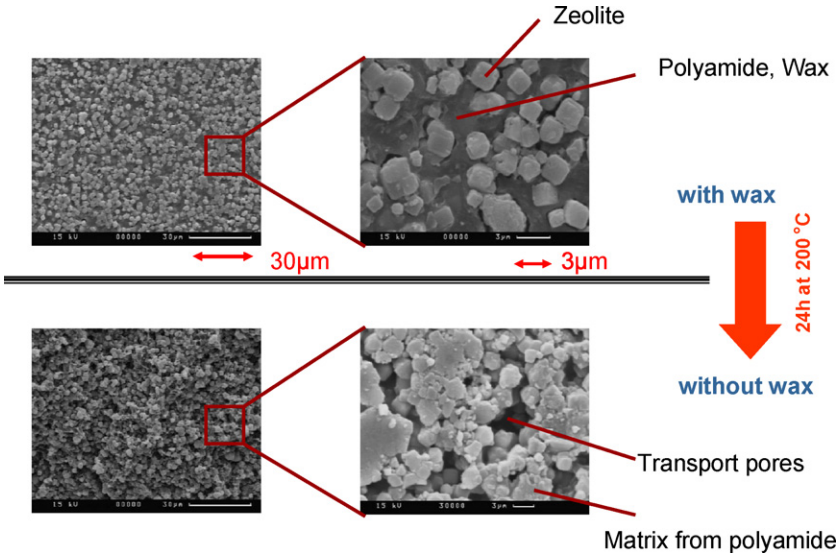


Fig. 2. SEM picture of the monolith before and after its thermal treatment [1].

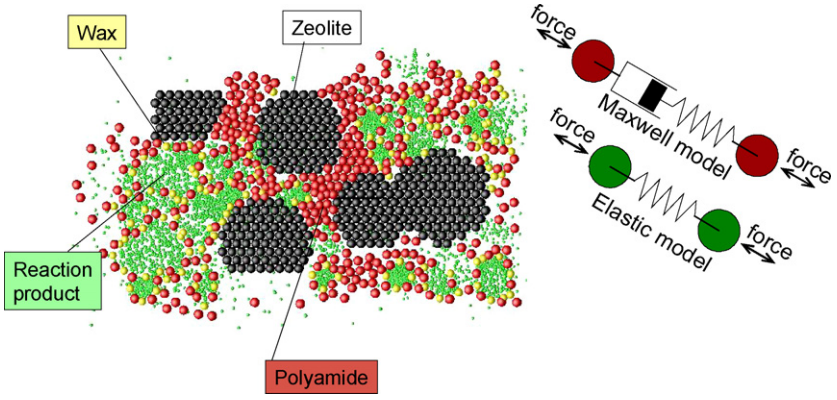


Fig. 3. Schematic drawing of the discrete element model (DEM) of the monolith containing several types of spherical micro-elements: zeolite (black), wax (yellow), polyamide (brown) and gas-phase reaction products (green). Schematic representation of force interactions represented by Kelvin and Elastic models. (For interpretation of the references to color in this figure legend, the reader is referred to the web version of the article.)

monolith before and after the thermal treatment are shown in Fig. 2.

## 3. Discrete element model of the generation of the porous structure in the monolith

Here we introduce the model of the generation of the secondary pore structure in the adsorption monolith during its heating in the oven in the stream of air. The discrete element method (DEM) [5–7] has been employed for this purpose. When modeling evolution of complex structures, DEM is one of good choices. The discrete element representation of the adsorption monolith is essentially the agglomerate of spherical micro-elements of different types, cf. Fig. 3.

The considered types of micro-elements are: (i) porous zeolite, (ii) polyamide, (iii) wax, and (iv) gas-phase resulting from the burning of wax. Each micro-element is described by its position vector $\boldsymbol{x}_i=(x_i, y_i, z_i)$, by its velocity vector $\upsilon_i=(\upsilon_{xi}, \upsilon_{yi}, \upsilon_{zi})$, by its radius $r_i$, by the average concentration of oxygen at the micro-element $c_i$ and by the type of micro-element $t_i$.

The movement of the $i$th micro-element is governed by kinematics and by the second Newton's law

$$\frac{\mathrm{d}\boldsymbol{x}_i}{\mathrm{d}t} = \boldsymbol{\upsilon}_i, \tag{1}$$

$$\frac{\mathrm{d}(m_i\boldsymbol{\upsilon}_i)}{\mathrm{d}t} = \sum_j \boldsymbol{F}_{ij},$$

$$\text{where } j \in \{\text{connected neighboring micro-elements}\} \tag{2}$$

where $m_i$ is the mass of the $i$th micro-element and $\boldsymbol{F}_{ij}$ is the force by which the $j$th micro-element acts on the $i$th micro-element. The summation is carried out over all binary force interactions with the neighbors of the $i$th micro-element. In addition, the contribution from ternary forces (e.g., the resistance to bending) can be included in Eq. (2), cf. our previous work [6,7].

During the thermal treatment of the monolith in the oven the volume fraction of the wax decreases and the volume fraction of the gaseous products of wax oxidation increases. This process is simulated by the shrinking of micro-elements of the type wax and by the formation of new micro-elements of the type gaseous reaction product. The gradual shrinking of the micro-element of wax by the burning in oxygen is described by the mass balance

$$\frac{\mathrm{d}m_i}{\mathrm{d}t} = \rho_{\mathrm{wax}} 4\pi r_i^2 \frac{\mathrm{d}r_i}{\mathrm{d}t} = -kc_i \left(\frac{4}{3}\right) \pi r_i^3 M_{\mathrm{wax}}, \quad t_i = \text{wax}, \tag{3}$$

where $k$ is the reaction rate constant and $c_i$ is the concentration of oxygen. The oxidation reaction $-CH_2- + (3/2)O_2 \rightarrow CO_2 + H_2O$ is assumed to occur only in wax micro-elements, and $M_{\mathrm{wax}}$ is the molar mass of one $-CH_2-$ group as the representative building block of the wax. While the volume of wax phase micro-elements decreases during the treatment of the monolith in the oven, new micro-elements of the gaseous product of burning are formed. Initial radius of wax elements was set to $r_i(0) = 0.1$ μm, so that the monolith structure (represented by SEM image) is discretized into computationally feasible number of micro-elements.

The balance of oxygen in the $i$th micro-element is governed by the equation

$$\frac{\mathrm{d}(c_i V_i)}{\mathrm{d}t} = \sum_j N_{ij} - \left(\frac{3}{2}\right) kc_i V_i, \tag{4}$$

where $V_i = (4/3)\pi r_i^3$ is the volume of $i$th micro-element, $N_{ij}$ is the molar flux of oxygen to the $i$th micro-element from its neighboring micro-elements and coefficient (3/2) stands for the stoichiometry of the oxidation reaction. In order to make the computational time shorter the transport and reaction of oxygen described by Eq. (4) is assumed to be in pseudo-stationary state, i.e., the left hand side of Eq. (4) is set to zero. The transport of oxygen through micro-elements of various types is assumed to proceed by the simple Fick's diffusion

$$N_{ij} = D_{ij}(c_j - c_i)\frac{A_{ij}}{\delta_{ij}}, \tag{5}$$

where $D_{ij}$ is the binary diffusion coefficient depending on the type of connected micro-elements, $A_{ij} = \pi(r_i^2 + r_j^2)/2$ is the assumed contact area and $\delta_{ij}$ is the distance of the $i$th and the $j$th micro-elements, respectively.

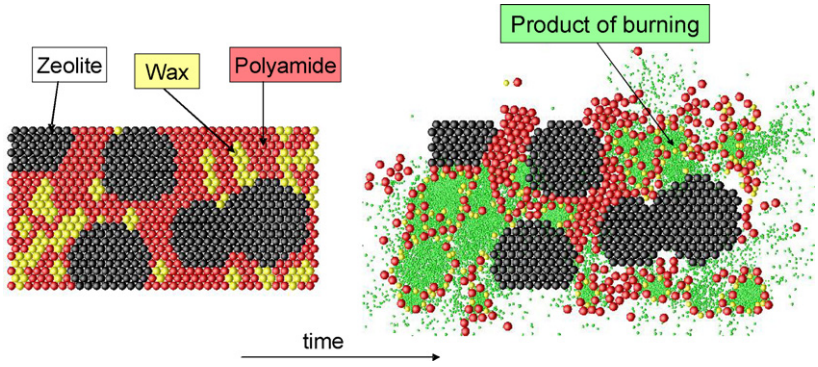


Fig. 4. The gradual shrinking of the wax phase and its replacement by the gas-phase in the adsorption monolith during its treatment in the oven. The considered monolith is discretized into interacting micro-elements by the discrete element method (DEM). The diameter of one micro-element is 0.2 μm.

At the beginning of our simulations there is one micro-element of the type reaction product with very small diameter attached to each micro-element of the wax. The growth of this attached micro-element of gas-phase with radius $r_{i,\mathrm{gas}}$ is described by equation

$$4\pi r_{i,\mathrm{gas}}^2 \frac{\mathrm{d}r_{i,\mathrm{gas}}}{\mathrm{d}t} = k_\mathrm{g}\left(-4\pi r_{i,\mathrm{wax}}^2 \frac{\mathrm{d}r_{i,\mathrm{wax}}}{\mathrm{d}t}\right), \tag{6}$$

where $k_\mathrm{g}$ is the coefficient reflecting the volume increase due to the transition from the solid to the gas-phase $(\mathrm{d}V_{i,\mathrm{gas}}/\mathrm{d}t) = k_\mathrm{g}(-\mathrm{d}V_{i,\mathrm{wax}}/\mathrm{d}t)$. The radius of the attached micro-element of the gaseous reaction product increases until it reaches prescribed maximum size. At that moment the growth of this micro-element is stopped. At the same time the new small micro-element of the gas-phase is attached to the micro-element of wax and the whole process is repeated. The number of micro-elements in the simulated adsorption monolith thus gradually increases.

Binary visco-elastic interactions acting among individual micro-elements are considered. Binary force interactions represent the resistance against push and pull of two micro-elements. During the dynamic simulation of the evolution of the particle consisting from a large number of micro-elements, two micro-elements $i$ and $j$ become connected when they touch each other, i.e., the distance of their centers $u$ becomes $u \leq u_0$, where $u_0 = r_i + r_j$ is the equilibrium distance between these micro-elements. Two elements become disconnected if the elongation $e = u/u_0$ exceeds the maximum value $e_{\max}$, i.e., if $e > e_{\max}$.

The character of polymer material lies between two limiting concepts. The first one is the concept of the deformation of solids, formally represented by the elastic spring and described by the Hook's law. The second concept is the fluid with linear viscous behavior, which is formally represented by the viscous dashpot with viscosity $\eta$. For obtaining the realistic force interactions between micro-elements several combinations of viscous and elastic components were implemented in our model, particularly the purely elastic and the Kelvin models. Kelvin model consists of the elastic spring and the viscous dashpot connected in parallel, cf. Fig. 3. The equation describing the Kelvin model is obtained by the combination of Hook's law and Newtonian viscous flow

$$\sigma = Ee + \eta\frac{de}{dt}, \tag{7}$$

where $\sigma = F_{ij}/A_{ij}$ is the stress acting between two connected micro-elements. The binary force $F_{ij}$ has to be projected into the direction of vector $\boldsymbol{u}$ connecting the centers of neighboring micro-elements, so that vector $\boldsymbol{F}_{ij}$ required in Eq. (2) is formed. Kelvin model was employed only for the description of force interactions among micro-elements because of its simplicity and more realistic behavior in comparison with purely elastic interactions.

The repulsive force interactions among gaseous micro-elements and their increasing number cause the increase of "pressure" in cavities containing gas-phase and subsequent formation of ruptures in the polyamide matrix. The secondary

Table 1
Force and transport connections between individual micro-elements

| Connection | Type of interaction | $E_{\mathrm{atr}}$ (Pa) | $E_{\mathrm{rep}}$ (Pa) | $e_{\max}$ | $(\eta_\mathrm{K}/E)$ ($\mathrm{s}^{-1}$) | $D_{ij}$ ($\mathrm{m}^2\mathrm{s}^{-1}$) |
|---|---|---|---|---|---|---|
| Wax–wax (W–W) | Kelvin | $10^3$ | $5\times10^5$ | 1.50 | 100.0 | $10^{-12}$ |
| Wax–gas-phase[a] (W–G) | Kelvin | $10^3$ | $10^4$ | 1.01 | 100.0 | $10^{-12}$ |
| Wax–polyamide (W–PA) | Kelvin | $10^3$ | $5\times10^5$ | 1.50 | 100.0 | $10^{-12}$ |
| Wax–zeolite (W–Z) | Kelvin | $10^3$ | $5\times10^5$ | 1.50 | 100.0 | $10^{-12}$ |
| Gas–gas-phase (G–G) | Kelvin | $10^2$ | $10^5$ | 1.01 | 100.0 | $10^{-6}$ |
| Gas-phase–polyamide (G–PA) | Kelvin | $10^3$ | $10^4$ | 1.01 | 100.0 | $10^{-12}$ |
| Gas-phase –zeolite (G–Z) | Kelvin | $10^3$ | $10^4$ | 1.01 | 100.0 | $10^{-12}$ |
| Polyamide– polyamide (PA–PA) | Kelvin | $10^3$ | $5\times10^5$ | 1.50 | 100.0 | $10^{-12}$ |
| Polyamide–zeolite (PA-Z) | Kelvin | $10^3$ | $5\times10^5$ | 1.50 | 100.0 | $10^{-12}$ |
| Zeolite–zeolite (Z–Z) | Kelvin | $10^3$ | $5\times10^5$ | 1.50 | 100.0 | $10^{-12}$ |

[a] Gas-phase represents the product of wax oxidation or the micro-elements of oxygen (cf. Fig. 8).

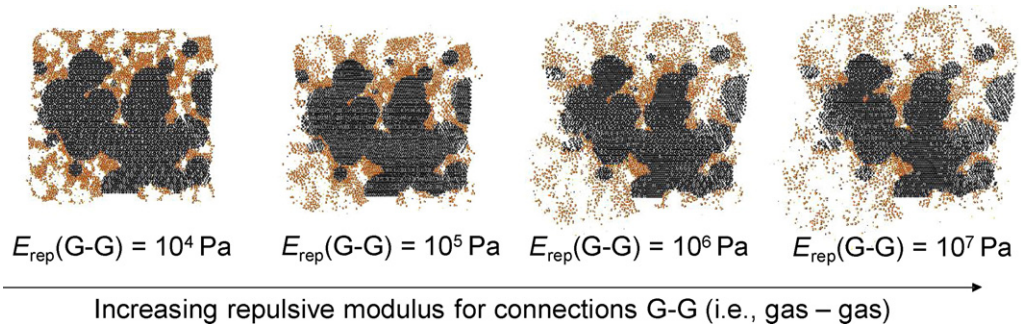


Fig. 5. Parametric study—increasing repulsive modulus between gas-phase micro-elements, i.e., increasing pressure of gas-phase micro-elements.

porous structure thus consists from areas filled by the gaseous phase micro-elements and from the void space in ruptures of the polyamide phase.

Fig. 4 presents an example structure of the adsorption monolith discretized into several types of micro-elements. For the sake of simplicity, mass transport resistances (to diffusion of oxygen) were not considered in the simulation shown in Fig. 4. Force interactions acting among individual micro-elements depend on the types of connected micro-elements (zeolite, polyamide, wax, product of burning). Classification of force interactions between micro-elements with respect to their types and analogous classification of transport (i.e., oxygen diffusion) connections is summarized in Table 1. Each connection is characterized by five parameters—the Young modulus for attraction $E_{atr}$ and repulsion $E_{rep}$ of micro-elements, maximum elongation of connected micro-elements $e_{max}$, the parameter $(\eta_K/E)$ used in the case of Kelvin visco-elastic interaction and binary diffusion of oxygen between connected micro-elements. Large value of repulsive modulus $E_{rep}$ prevents the inter-penetration of micro-elements.

Values of parameters summarized in Table 1 were set somewhat arbitrarily, but shall qualitatively reflect the real behavior of materials. Mechanical (elastic) properties of polymeric materials (polyamide and wax) are usually reported at temperature 25 °C. Elastic and visco-elastic properties at 200 °C can be only qualitatively estimated. The results of our simulations are therefore not expected to agree quantitatively with experimentally obtained morphologies. The values of elastic moduli $E_{atr}$ and $E_{rep}$ are reduced by several orders of magnitude from their real values to make the simulations computationally feasible while not affecting the morphology evolution [6]. Diffusion coefficients reflect different rates of diffusion in gas and solid-phases.

## 4. Results

Here we perform simulations of the type "proof-of-the-concept" and demonstrate, that even such simulations can provide us with qualitative guidance on the effect of processing parameters with respect to the final morphology of the monolithic adsorbent.

Two examples of simple parametric studies are provided in Figs. 5 and 6, respectively. The damage of the original polyamide phase due to the oxidation of wax and the expansion of gaseous reaction products depends on the repulsive Young modulus of the connection of micro-elements gas-phase–gas-phase (Fig. 5) and on the repulsive Young modulus between micro-elements of the solid-phase (Fig. 6). Although the uncertainty in values of model parameters is large, we can observe the robust evolution of the secondary porous structure. The change of repulsive elastic moduli by an order of magnitude causes only small difference in the resulting porous structure.

The effect of the content of wax in the polyamide matrix on the resulting porosity generated during the oxidation of wax is shown in Fig. 7. The middle column displays the initial structures containing different fractions of wax and polyamide phases and the specification of these structures is reported in Table 2. The left and right columns in Fig. 7 show the same resulting struc-

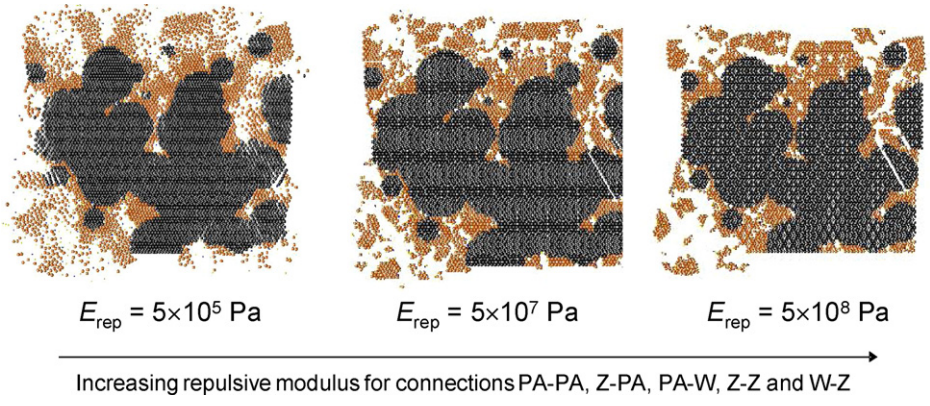


Fig. 6. Parametric study—increasing repulsive modulus between solid-phase micro-elements.

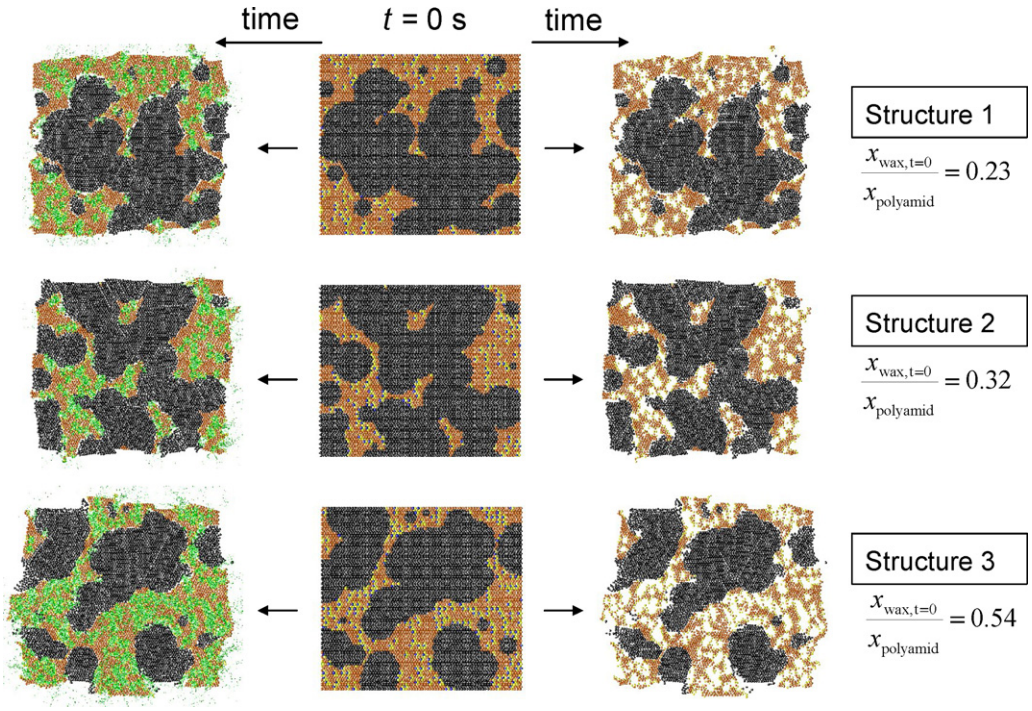


Fig. 7. Effect of the different contents of the wax within the polyamide matrix on the resulting secondary porous structure, cf. Table 2. Gas-phase micro-elements are displayed in the left and are not displayed in the right column.

tures after some wax was removed by burning. The right column without the green micro-elements of the gaseous reaction product is provided to make the final porous structure more clear. The porosities of the resulting structures presented in Fig. 7 were evaluated and are summarized in Table 2. Resulting structures 1 and 2 show that the generated porosity can be higher then the volume fraction of the wax phase present in the initial monolith due to the deformation of polyamide and zeolite phases. Fig. 8 then demonstrates the growing number of zeolite macro-elements accessible through the generated secondary pores. Fig. 7 demonstrates just a few initial structures of adsorption monolith. More simulations can be carried out either from SEM images directly discretized into micro-elements or by the evaluation of statistical descriptors from SEM images and subsequent generation of initial structures.

Simulations of the formation of the secondary porous structure in the monolithic adsorbent can be performed also in spatially 3D cases, cf. Fig. 9. The bottom row in Fig. 9 shows the resulting structure omitting micro-elements of the solid-phase, green micro-elements of the gas-phase are present in the pores. The porous structure within adsoprtion monolith can thus be observed. The simulation time is considerably larger in the case of spatially 3D simulations due to the large number of micro-elements and connections between neighboring micro-elements. The final number of micro-elements for the structure displayed in Fig. 9 is approximately 15 000. The average coordination number of micro-elements (i.e., the number of connected neighbors) in spatially 3D simulations is larger than in spatially 2D cases, hence the polyamide phase in the 3D case is not fragmented into large number of pieces as is the case of 2D simulations.

No resistance against the transport of oxygen to the micro-elements of the wax phase was considered in the results presented so far, hence the uniform concentration of the oxy-

Table 2
Characterization of three monolith structures, $x$ is the volume fraction and $\varepsilon$ is the porosity

| | $x_{zeolite}$ | $x_{polyamide}$ | $x_{wax}$ | $\varepsilon$ |
|---|---|---|---|---|
| Structure 1 | 0.63 | 0.30 | 0.07 | 0.171 |
| Structure 2 | 0.71 | 0.22 | 0.07 | 0.177 |
| Structure 3 | 0.60 | 0.26 | 0.14 | 0.240 |

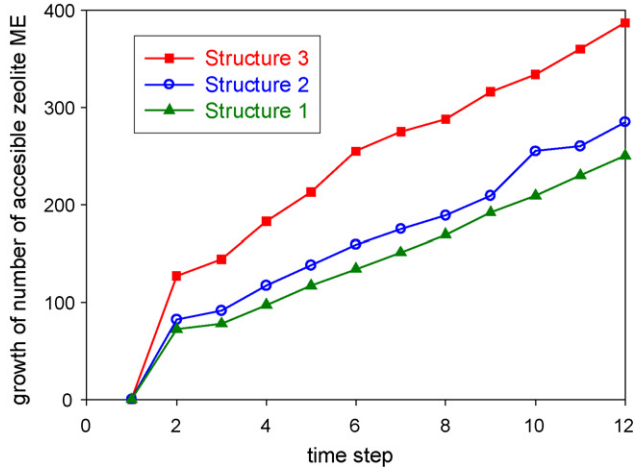


Fig. 8. Growth of the number of zeolite micro-elements accessible through newly formed macro-pores in the generated secondary porous structure, cf. corresponding Fig. 7 and Table 2.

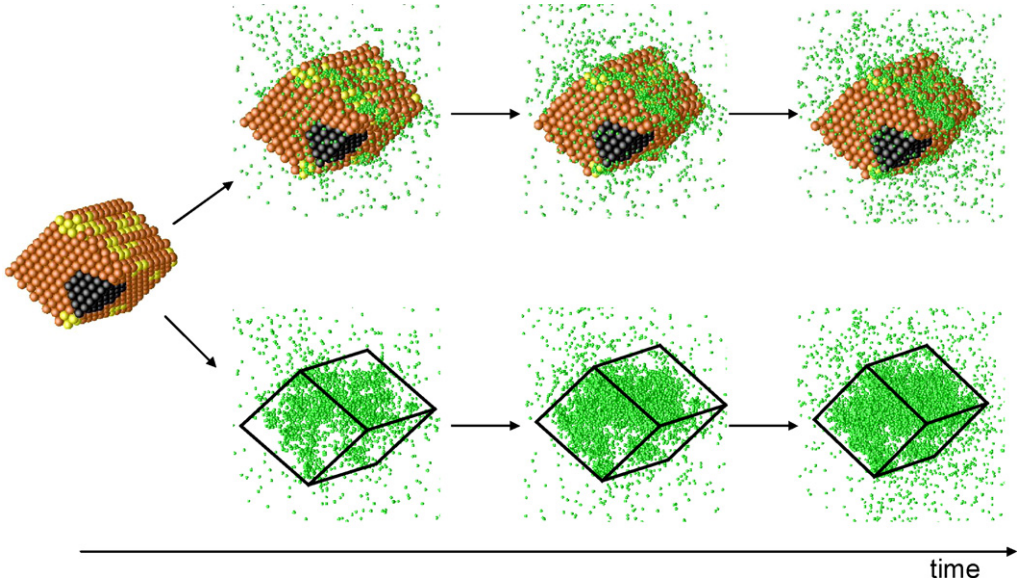


Fig. 9. Spatially 3D simulation of the formation of the secondary porous structure in the adsorption monolith.

gen was considered. Let us now consider the case of the limited diffusion transport of oxygen to wax micro-elements. In this case micro-elements of gas (containing oxygen) are introduced also outside the simulated structure of the monolith. Moreover, diffusion transport in the monolith structure is considered among all types of connected micro-elements.

The example of the formation of the porous structure in the case of the limited diffusion transport of oxygen is presented in Fig. 10. The sequence of images in Fig. 10a shows the evolution of the monolith structure, the shrinking of wax micro-elements and the formation of the new micro-elements representing the gaseous product of wax oxidation. The oxygen is assumed to be transported to the lower boundary of the monolith structure, and therefore the rate of wax burning is largest close to this boundary. The sequence of images in Fig. 10b displays the evolution of the concentration profile of oxygen in the monolith and in the gas-phase located close to the lower boundary. Red color here represents high concentration of oxygen and the dark blue color represents the low concentration of oxygen. Micro-elements below the monolith in Fig. 10b represent the gas-phase

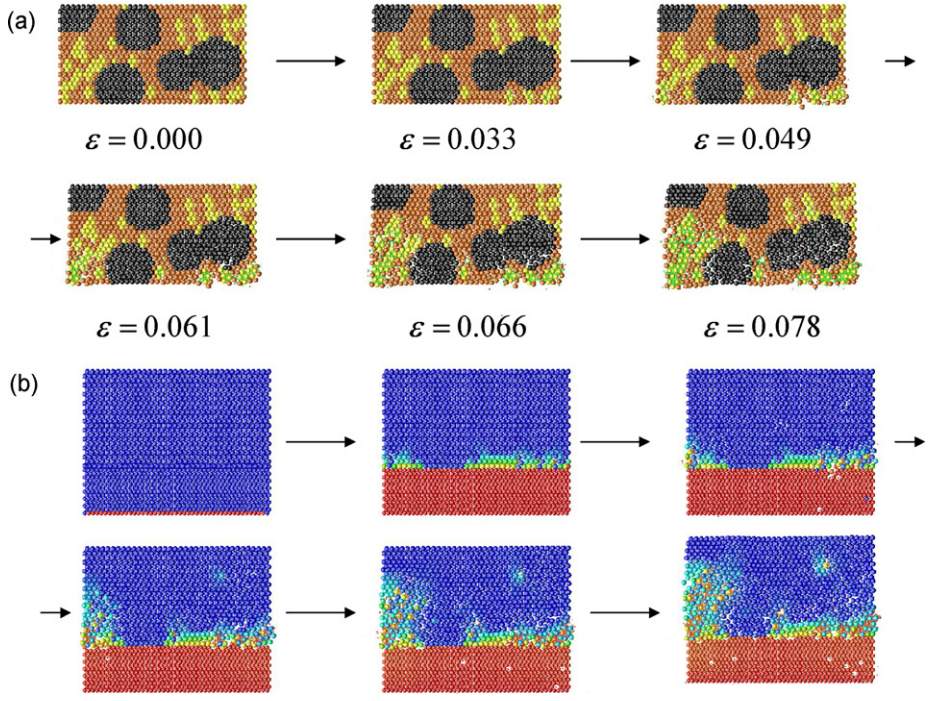


Fig. 10. Gradual removal of the wax phase from the adsorption monolith in the case of limited diffusion transport of oxygen. (a) Evolution of the structure of the monolithic adsorbent, (b) evolution of the concentration field of oxygen (red color represents high and blue color low concentration of oxygen). (For interpretation of the references to color in this figure legend, the reader is referred to the web version of the article.)

containing oxygen. As the wax in the outer layer of the monolith is converted into the gaseous products the secondary pores are gradually formed and allow the faster diffusion of oxygen to the wax micro-elements located deeper in the monolith structure. The oxidation of wax displayed in Fig. 10 is diffusion-limited as the oxidation reaction is relatively fast. Oxygen concentration in the wax phase located deep in the monolith (far from the surrounding gas-phase) is low due to the diffusion control of the oxidation of wax.

Fig. 10 was obtained with model parameters slightly different from those reported in Table 1. Maxwell force interactions with relaxation time $\tau_{rel} = 1$ s were considered for connections between solid micro-elements, while elastic interactions were assumed for gas–solid interactions. The same values of attractive and repulsive elastic moduli have been employed. Maximum elongation for connections solid–gas and gas–gas is $e_{max} = 1.5$ and for connections solid–solid is $e_{max} = 1.25$.

## 5. Conclusions

During the manufacturing of monolithic adsorbents a secondary porous structure has to be generated (e.g., by the thermal treatment) in order to allow fast mass transfer of adsorbates to zeolite crystals. A rigorous description of the thermal treatment of the monolith would involve the simultaneous calculation of stresses in the solid-phase, transport of gaseous reactants and products, oxidation of the wax phase and formation of blowing agents in the evolving multi-phase structure. Modeling of such a rigorous description is hardly feasible. Therefore we developed a simplified approach based on the discrete element method with micro-elements of several types (zeolite, polyamide, wax, gas-phase) with mutual force interactions and diffusion of gaseous species acting among the connected micro-elements and with the wax oxidation taking place in the respective micro-elements. Such DEM-based model is capable to predict the formation of cracks in the polyamide phase and of the secondary porous structure in the adsorption monolith.

Nowadays the chemical engineering simulations have to be capable to predict not only spatial distributions of concentrations, velocity, temperature and pressure fields, but also predict the generated complex spatially 3D morphology of products and to estimate application properties of these products. This contribution demonstrates how the approximate first-principles based model can aid in the predictive modeling and understanding of the evolution of porous structure in the complex case of multi-phase media composed of four different phases. Application properties of the generated porous/multi-phase media can then be estimated, e.g., by the concept of reconstructed porous media [8].

Because the parametric space of the problem is wide and values of some parameters are not available at typical conditions of thermal treatment, we performed several parametric studies and demonstrated robustness of our model. Refinement of simulation results is well possible with the help of a more detailed experimental input. Systematic parametric studies can provide us with the qualitative guidance on the effects of processing parameters and the initial distribution of polyamide and wax phases on the final morphology of the monolithic adsorbent. However, achievement of the quantitative agreement of modeling results with experiments is not anticipated in the near future.

## Acknowledgments

The support from the European high performance computing project RII3-CT-2003-506079 and from the Czech grant agency (104/07/1127) is acknowledged.

## References

[1] A. Gorbach, M. Stegmaier, J. Hammer, H.-G. Fritz, Compact pressure swing adsorption—impact and potential of new-type adsorbent-polymer monoliths, Adsorption 11 (2005) 515–520.
[2] H.-G. Fritz, J. Hammer, Aufbereitung zeolitischer Formmassen und ihre Ausformung zu Adsorptionsformteilen, Chemie Ingenieur und Technik 77 (2005) 1587–1600.
[3] A. Gorbach, M. Stegmaier, G. Eigenberger, Measurement and modelling of water vapor adsorption in zeolite 4A, Adsorption 10 (2004) 29–46.
[4] J. Hammer, Entwicklung zeolithischer Adsorptionsformteile mit thermoplastischen Polymeren als Plastifizier- und Bindemittel, in: Dissertation, Institut für Kunststofftechnologie, Universität Stuttgart, 2005.
[5] D.M. Heyes, J. Baxter, U. Tüzün, R.S. Qin, Discrete element method simulations: from micro to macro scales, Philos. Trans. Royal Soc. A 362 (2004) 1853–1865.
[6] Z. Grof, J. Kosek, M. Marek, Modeling of morphogenesis of growing polyolefin particles, AIChE J. 51 (2005) 2048–2067.
[7] Z. Grof, J. Kosek, M. Marek, Principles of morphogenesis of polyolefin particles, Ind. Eng. Chem. Res. 44 (2005) 2389–2404.
[8] J. Kosek, F. Stepanek, M. Marek, Modeling of transport and transformation processes in porous and multiphase bodies, in: G.B. Marin (Ed.), Advances in Chemical Engineering, "Multiscale Analysis", 30, Elsevier, 2005, pp. 137–203.